

# Flow-based Autoregressive Structured Prediction of Human Motion

Mohsen Zand

m.zand@queensu.ca

Ali Etemad

ali.etemad@queensu.ca

Michael Greenspan

michael.greenspan@queensu.ca

Department of Electrical and Computer Engineering, Ingenuity Labs  
Queen's University, Kingston, ON, Canada

## Abstract

A new method is proposed for human motion prediction by learning temporal and spatial dependencies in an end-to-end deep neural network. The joint connectivity is explicitly modeled using a novel autoregressive structured prediction representation based on flow-based generative models. We learn a latent space of complex body poses in consecutive frames which is conditioned on the high-dimensional structure input sequence. To construct each latent variable, the general and local smoothness of the joint positions are considered in a generative process using conditional normalizing flows. As a result, all frame-level and joint-level continuities in the sequence are preserved in the model. This enables us to parameterize the inter-frame and intra-frame relationships and joint connectivity for robust long-term predictions as well as short-term prediction. Our experiments on two challenging benchmark datasets of Human3.6M and AMASS demonstrate that our proposed method is able to effectively model the sequence information for motion prediction and outperform other techniques in 42 of the 48 total experiment scenarios to set a new state-of-the-art.

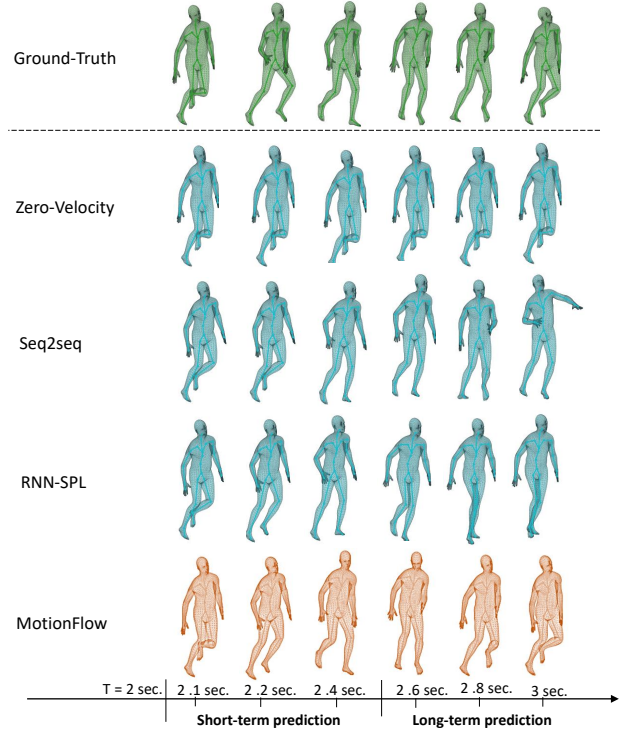


Figure 1: Motion prediction for a sequence from AMASS dataset [33]. From top to bottom, we show the ground truth, the results of Zero-Velocity [35], Seq2seq [35], RNN-SPL [2] and our method (MotionFlow). The results show that our method can maintain temporal and spatial smoothness in the target motions in both short-term and long-term prediction considerably better than the other methods.

## 1. Introduction

Automated prediction of human motion is a challenging task due to the inherent dynamic and stochastic nature, non-linearity, high dimensionality, and complex context dependency of motion. Human motion prediction is an essential task in computer vision with many useful applications in autonomous driving, human robot interaction, and health-care [14, 35].

Current state-of-the-art methods mainly rely on Recurrent Neural Networks (RNNs) with the aim of modeling contextual information in the temporal dimension via motion-based dynamics [55, 2]. The performance of RNNs

however relies on the effectiveness of the extracted spatial skeleton features. RNNs also tend to overemphasize on the temporal information in the data stream, which can lead to overfitting, especially when the training data is insuffi-

cient [53].

When modeling structured human motion, the position of the joints in the predicted frames generally do not rely solely on the temporal smoothness [14] which results from temporal dependencies. Rather, the bio-mechanical dynamics of human motion are critical to encourage local smoothness of the sequences. Spatial configuration has been recently leveraged by motion prediction models, resulting in performance improvements [14, 34, 5]. Thus, motion prediction is treated as a multi-output problem and the spatial dependencies between the joints are encoded using different structured prediction algorithms. Recent examples of structured output applied to human motion prediction include [47] and [28].

Recently, flow-based generative methods have shown promising performance in modeling complex outputs [40, 36, 24, 16]. These models are based on normalizing flows, a family of generative models with tractable distributions that consist of invertible components [26]. Flow-based methods have been applied to non-temporal data such as images, and are limited in their ability to effectively modeling complex interactions in structured outputs [25, 40, 56]. Nonetheless, we believe their ability to learn multi-output distributions makes them particularly attractive for human motion prediction.

To learn more robust spatio-temporal representations while maintaining the structure of high-dimensional human motion data, we introduce *MotionFlow*, a flow-based generative structured prediction model designed for motion prediction. Specifically, our method is a conditional autoregressive flow-based solution which can directly model the log-likelihood of temporal and spatial data for arbitrarily long sequences. This enables both short-term and long-term prediction of motion more accurately since the local smoothness compensates for prediction discontinuities in longer sequences. Figure 1 illustrates the proposed method is able to maintain temporal and spatial smoothness for both short-term and long-term predictions. We evaluate our method by performing extensive experiments and ablation studies on H3.6M [20] and AMASS [33], and illustrate that **MotionFlow** outperforms other methods in the field by generating more accurate and consistent predictions.

Our contributions are summarized as follows. (1) We propose a novel structured prediction algorithm to generate structured outputs conditioned on input and output variables. Our model is different from existing works in that it can model both spatial (intra-frame) and temporal (inter-frame) dependencies for high-dimensional data with conditional flow-based generative models. (2) We apply our method to the challenging task of motion prediction and demonstrate that our model is able to leverage normalizing flows to learn human motion using the observed frames and spatial structure to predict the future instances of mo-

tion. (3) We perform extensive experimental evaluation on two widely used challenging datasets and show the effectiveness of the proposed method for skeleton-based motion prediction by setting a new state-of-the-art.

## 2. Related work

Our method relates to the topics of motion modeling, structured prediction, and flow-based representation learning. We briefly review the most relevant related literature in the following subsections.

### 2.1. Human motion modeling

In several previous methods, sequential joint features were modeled using different variations of recurrent neural networks (RNNs) given their ability to learn time series [52, 11]. For instance, Martinez *et al.* [35] developed a sequence-to-sequence architecture with residual connections by applying changes such as sample-based loss to the standard RNN. Comprehensive motion modeling, however, requires both spatial and temporal reasoning, while RNN-based methods are generally unable to model the spatial relationships between the joints.

Leveraging the structure and spatial relationships between joints has recently shown encouraging results, suggesting the significance of the connectivity. For instance, Du *et al.* [10], split the human skeleton into five body parts based on the physical structure of the human body. These were then fed into five bidirectional RNNs to automatically learn a multi-level representation of skeletal data. In [55], an RNN model using a deep Long Short-Term Memory (LSTM) network was developed for skeleton-based action recognition. Their deep LSTM network modeled co-occurrences between joints. The approach of Shahroury *et al.* [43] considered human activities as interactions of different body parts and developed a part-aware LSTM model for action recognition. They utilized long-term temporal correlations for each body part and split the memory cell of the LSTM into part-based sub-cells. These methods, however, are mostly based on hand-crafted rules for incorporating spatial features. Mao *et al.* [34] recently proposed to tackle discontinuities in motion prediction by encoding temporal information in trajectory space, instead of the pose space.

### 2.2. Structured prediction

A variety of approaches have been studied for modeling structures between output variables [4, 50, 12, 32]. These methods are mainly a generalization of the standard classification algorithms such as conditional random field (CRF) [46], structured SVM (SSVM) [49], and structured perceptron [6] to model the correlations between output variables. Belanger and McCallum [4] proposed structured prediction energy networks (SPENs) which used an energy

function for scoring structured outputs. Gradient descent was then used to optimize the assigned energies with respect to the ground-truth outputs. Graber *et al.* [12] proposed the use of output variables as an intermediate structured layer between deep neural structure layers to capture non-linear interactions among output variables. Graber and Schwing [13] presented graph structured prediction energy networks to better model local and higher-order correlations between output variables. An exact inference for structured prediction is however NP-hard. Thus, different types of prediction regularization [37] and approximate inference [15, 50] have been developed.

An approach that is close to our work is [2], where a structured prediction layer was introduced to model the joint dependencies given motion context (*i.e.*, a neural representation of the past frames). The prediction at the final stage was decomposed into individual joints using separate small networks. The goal in structured prediction, however, is to learn a function between the input and the structured output space [38, 4]. Although this approach models the hierarchical structure of the body joints, learning the spatial dependencies is decoupled from the temporal relationships. In contrast, our method is a deep conditional generative model which generates the joint positions in the future frames by simultaneously considering sequence-level, frame-level, and joint-level continuity from local and global perspectives.

### 2.3. Flow-based representation

Normalizing Flows have been successfully explored as a family of generative models with tractable distributions [3, 17, 27, 26]. A Normalizing Flow is a transformation of a simpler probability distribution into a more complicated distribution by a sequence of invertible and differentiable functions. Many applications based on normalizing flows have recently emerged in the literature, such as density estimation [8], variational inference [42], image generation [24], and noise modelling [1]. For a comprehensive review of this concept, we refer the reader to [26].

Flow-based generative models have also been investigated for complex outputs. Dinh *et al.* [9] proposed real-valued non-volume preserving (real NVP) transformations to model high-dimensional data. They used invertible and learnable transformations for exact sampling, inference of latent variables, and log-density estimation of data samples. Kingma and Dhariwal [24] proposed ‘Glow’ as a generative flow by leveraging more invertible layers. They used invertible  $1 \times 1$  convolutions in their model and employed it to synthesize high-resolution natural images. In [16] a method called Flow++ further improved the generative flows using variational dequantization and architecture design. It is a non-autoregressive model for unconditional density estimation. Hoogeboom *et al.* [17] proposed emerging con-

volution by chaining specific autoregressive convolutions which were invertible with receptive fields identical to standard convolution.

In this work, we extend flow-based generative models into the setting of autoregressive conditional structured output learning for motion prediction. We specifically propose a new generative model which is conditioned on spatio-temporal dependencies of the input elements for learning high-dimensional structured outputs.

## 3. Proposed method

### 3.1. Problem formulation

Let  $X = \{q_1, \dots, q_T\}$  denote a motion sequence where each frame  $q_t \in \mathbb{R}^{J \times H}$  represents a human body pose at time  $t$ , with  $J$  number of joints in the skeleton, and each joint with  $H$  dimensions. The dimensions of each joint can minimally be  $H = 3$  indicating a pure 3D translational representation of each joint, or can more generally include a rotational component indicating the orientation of a coordinate reference frame centered at each joint [2], represented as a matrix ( $H = 9$ ), angle-axis ( $H = 3$ ), or quaternion ( $H = 4$ ). Thus, each joint  $j$  at time-step  $t$  can be represented by  $q_t^j \in \mathbb{R}^H$ .

We formulate structured prediction of motion as follows. Let the body joint positions at  $q_t$  be estimated using the sequence of  $t-1$  previous joint positions at  $\{q_1, q_2, \dots, q_{t-1}\}$ . The goal is to model a mapping from input poses at time-steps  $i = 1, \dots, t-1$  to a high-dimensional structured output consisting of poses at frame  $t$ . More specifically, we represent the input and output sequences to our model as  $x = \{q_i\}_{i=1}^{t-1}$  and  $y = \{q_i\}_{i=2}^t$ , respectively. Each  $y_i = q_i = \{q_i^1, \dots, q_i^J\}$  denotes the motion vector at time  $i$  comprising  $J \times H$  joint values.

### 3.2. Our method: MotionFlow

We propose a novel autoregressive generative structured prediction model using normalizing flows. Given a training set of multi-variate input-output pairs  $\{(x, y)\}$ , where  $x$  is a structured input sequence and  $y$  denotes its corresponding ground-truth structured output, we use conditional normalizing flows to model the conditional distribution  $p(y|x)$ . To approximate this distribution, each frame  $q_i$  must be conditioned on the previous frames to maintain temporal smoothness. Moreover, each joint position depends on the positions of all other joints in the current frame. The motion prediction task therefore requires the simultaneous modeling of higher order temporal dependencies and spatial connectivities between output variables. These form the intuition behind the autoregressive nature of our approach. To this end, we expand and extend existing techniques to accommodate both *intra-frame* spatial and *inter-frame* spatio-temporal joint relationships.

To tackle the high dimensionality of human motion, we propose to condition the output on the input variables using a flow-based model. The predictive process of the output can then be modeled using a conditional true distribution  $p^*(y|x)$  which can be approximated with a model  $p(y|x, \theta)$  that maximizes the data likelihood, *i.e.* by minimizing the following negative log-likelihood expression:

$$-\frac{1}{N} \sum_{i=1}^N \log p(y_i|x_i, \theta), \quad (1)$$

where  $N$  denotes the number of samples in the dataset, and  $\theta$  is the model parameter.

An overview of our method is represented in Figure 2, where  $y$  is modeled by latent variable  $z_L$  through conditioning  $y$  on input  $x$ . Our method consists of two main modules, *i.e.* normalizing flow and conditioning module, where the conditioning uses input sequences for output generation by means of normalizing flow. In the following, we describe these two modules.

### 3.2.1 Normalizing flows

Normalizing flows are desirable solutions to address one-dimensional regression problems [26]. In the steps of normalizing flow, a latent representation of the output is learned by initializing a base distribution. The base distribution  $p_0(z_0)$  is transformed to a more complex density  $p_K(z_K)$  iteratively using a generator function  $g$ . The inverse function  $f = g^{-1}$  can move (*‘flow’*) in the opposite direction from the base distribution. Here,  $f$  implies one step of the flow with different neural network layers. The inference can be performed and a complex distribution can be obtained from the simple base distribution. In our motion prediction task, however, our outputs are high-dimensional structured tensors. As shown by Trippe and Turner [48], conditional distributions are *‘similar’* if the observed variables are *‘similar’*, *i.e.*:

$$x_i \approx x_j \Rightarrow p(y|x_i) \approx p(y|x_j) \quad (2)$$

In normalizing flows, distributional similarity can be defined as closeness in the parameter space. One interesting point is that placing priors on this distribution can control the amount of expansion and contraction of the base distribution in each step of the normalizing flow. Intuitively, tunable priors can be used over weights and bias parameters to map them from the hidden layers to the parameters of the normalizing flow. This strategy is efficient for solving a one-dimensional regression problem [48]. It has also been utilized for multi-output learning [32]. This concept can be generalized in conditional normalizing flows where  $f = f_1 \circ f_2 \circ \dots \circ f_M$  is defined as a composition of  $M$  bijective functions. It can potentially be represented

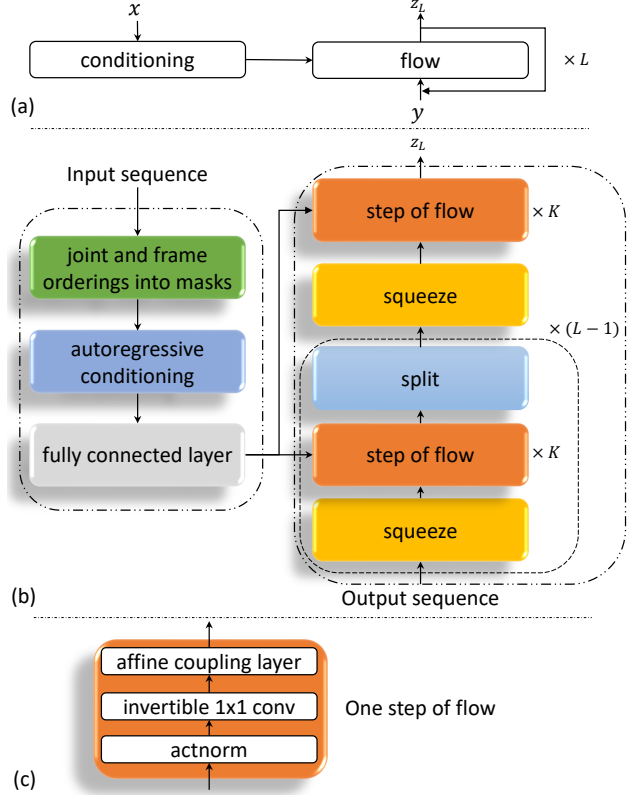


Figure 2: Overview of our model. (a) MotionFlow uses a conditioning module to leverage the generation process of the high-dimensional output sequence using a given input sequence. (b) The output sequence is encoded into multiple latent variables in a multi-scale flow structure. The conditioning module applies joint and frame ordering masks to convolution operations and provides scale and bias parameters to initialize the conditioning for each step of the Glow network. (c) One step of flow in the Glow architecture is represented.

as  $f = f_{x, \phi_1} \circ f_{x, \phi_2} \circ \dots \circ f_{x, \phi_M}$ , where each function  $f_{x, \phi_i}$  is parameterized by both  $x$  and  $\phi_i$ . One interesting result is that each  $\phi_i$  can be an autoregressive model with arbitrary conditionals. The following conditional likelihood can then obtain the likelihood-based estimation of the parameters:

$$\log p(y|x, \theta) = \log p_Z(z) + \sum_{i=1}^M \log \left| \det \left( \frac{\partial f_{x, \phi_i}}{\partial h_{i-1}} \right) \right| \quad (3)$$

where  $z$  is the latent variable and  $p_Z(z)$  has a tractable density. In the second term,  $h_0 = x$ , and  $h_M = z$  which is recursively obtained by  $h_i = f_{\phi_i}(h_{i-1})$ . This allows us to use normalizing flows for structured prediction as per Eq. ???. We therefore place the priors over conditional distributions defined by normalizing flows, so that the changes in the input space impact the structured output. This can



be a neural network with  $x$  as its input that generates the parameter weights for each layer of the normalizing flow.

We use the popular multi-scale flow-based architecture Glow [24] in our proposed method. Each step of Glow consists of actnorm which stands for activation normalization, invertible  $1 \times 1$  convolution, and affine coupling operations. The *actnorm* operation calculates the affine transformation of the activations using scale and bias parameters for each channel. The *invertible  $1 \times 1$  convolution* is a generalization of a permutation operation. The *affine coupling* layer captures the correlations among spatial dimensions. It splits the input variables along the channel dimension into two halves. It then adds a learned transformation of one half to the other half [24, 32].

### 3.2.2 Conditioning module

The conditionals in motion prediction task are based on temporal and spatial connectivities, which are critical to maintain local and global smoothness. To predict the  $t^{th}$  frame, the inter-frame and intra-frame autoregressive models can be described as  $p(q_t|q_{1:t-1})$  and  $p(q_t^j|q_t^{1:j-1})$  respectively. The latter model is motivated by the fact that human motions are fundamentally regulated by the spatial structure of the skeleton [2]. The global interactions at the sequence level therefore depend on the spatial joint information. Formally, human motion consists of a sequence of human poses characterized by body joint positions or 3D-joint rotations [41]. Accordingly, human body is represented by a kinematic tree consisting of five kinematic chains: the spine and the four limbs, with a total of 57 DoFs [30].

In our model, we propose a conditioning module that includes: (1) a mask generation layer, (2) an autoregressive conditioning step, and (3) a fully connected layer. Mask generation is performed to transfer the frame and joint orderings into a number of weights as shown in Figure 3. This figure shows the orderings for 10 consecutive frames and 5 joints. In autoregressive conditioning step we use two convolution operations for inter-frame and intra-frame structures respectively. We use a frame-ordering mask (as shown in Figure 3 (a)) for the first convolution and a joint-ordering mask (as shown in Figure 3 (b)) for the second convolution. These orderings allow the model to generate each frame by conditioning the each frame on its past frames, while preserving joint spatial dependencies by enforcing the model to learn kinematic chain hierarchy. To apply the ordering masks on the joint positions, we adopt an autoregressive process similar to PixelCNN [39] which is used for conditional autoregressive image generation. Next, we apply fully connected (FC) layers to map the representations obtained by the convolution layers to determine the scale and bias parameters to initialize the conditioning for each

step of the Glow network. Therefore, there are 3 networks and each network includes two convolutional layers with 16 channels, kernel size 3 and stride 1. The input and output motion sequences to MotionFlow are in the form of matrices with shape  $[(t-1) \times (J \times H)]$ . We reshape this 2D representation into 3D to take advantage of 3D convolutions, and feed the motion matrices of shape  $[3 \times ((t-1)/3) \times (J \times H)]$  into our network. A fully connected layer then provides the parameterized conditions at each step of normalizing flow.

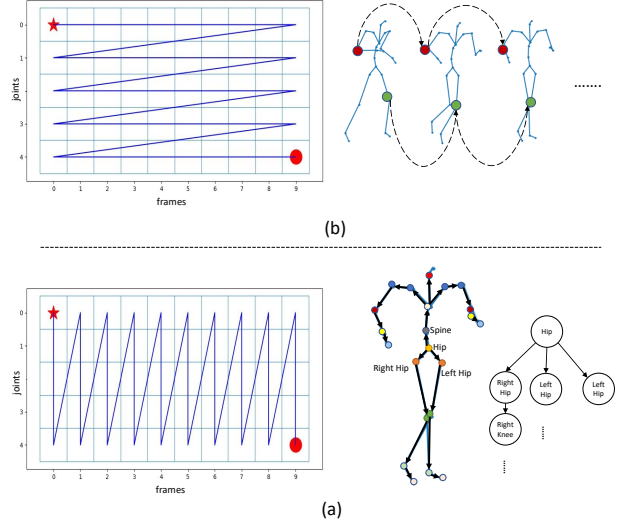


Figure 3: Mask orderings for convolutions. Frame ordering (a) and joint ordering (b) are encoded into corresponding masks. These masks provide autoregressive weights for the convolution operations in the conditioning module. \* and • show the starting point and the stopping point, respectively.

At inference time, we aim to predict the best output  $y^*$  for a given  $x$ . This can be formulated as  $y^* = \arg\max_y p(y|x)$ . The transformation function is first calculated using a given  $x$ . The latent variable  $z$  can then be modeled from  $p_Z(z)$  and propagated to obtain the corresponding output  $y$ . This procedure can be formulated as:

$$\begin{aligned} z &\sim p_Z(z) \\ y &= g_{x,\phi}(z) \end{aligned} \quad (4)$$

where  $g_{x,\phi} = f_{x,\phi}^{-1}$  denotes the inverse function.

We can use gradient-based optimization techniques such as gradient descent to optimize  $y$ . To avoid the local optima due to the multi-modality and non-convexity of the density distribution and to converge faster, we follow a sample-based approximate strategy for inference [32]. A set of samples drawn from  $p_Z(z)$  are defined as  $\{z_1, \dots, z_M\}$ . The output can then be estimated by averaging over these vari-

ables:

$$y^* \approx \frac{1}{M} \sum_{i=1}^M g_{x,\phi}(z_i). \quad (5)$$

Once the model parameters are learned, output  $y$  is predicted from an input  $x$  by following the generative process of the model:

$$y^* = \operatorname{argmax}_y p_\theta(y|x, z^*) \quad (6)$$

Once trained, our proposed model is capable of learning high-dimensional outputs with temporal and spatial interactions to predict future motions.

## 4. Experiments

We evaluate the quantitative and qualitative aspects of the proposed method on two challenging benchmark datasets, H3.6M [20] and AMASS [33]. We provide comparisons to previous state-of-the-art motion prediction techniques. We also present ablation experiments on the key components of our model to quantify their impact.

### 4.1. Experiment setup

#### 4.1.1 Datasets and protocols

**H3.6M.** Human3.6M [20] is a large dataset containing 3.6 million high quality 3D body joint positions, collected for 15 periodic and non-periodic actions performed by seven different professional actors. The video sequences are captured by a Vicon motion capture system and sampled at 50 frames per second (fps). At each frame, the 3D position of 32 body joints are captured, from which we choose 21 representative joints similar to [22, 35], and [2]. We train our model on 120 frames to predict the next 24 frames at inference for short-term prediction. This differs from other works which generally use 143 frames for training and predict the subsequent single frame [2].

**AMASS.** AMASS [33] is a more recent dataset consisting of multiple smaller publicly available motion datasets, *e.g.* HumanEva [44] and CMU Mocap [7]. It is a challenging dataset which provides many more ( $14\times$ ) samples than H3.6M captured for a diverse range of actions. It uses a skinned multi-person linear (SMPL) [31] model for motion representation. The dataset includes 8,593 clips consisting of 9,084,918 frames sampled at 60 fps. We use 90%, 5%, and 5% of all the clips for training, validation, and testing, respectively. We use 15 major joints for motion representation, as in [2]. The clips are divided into 144 frame sequences. The first 120 frames of each sequence are used for training while the following 24 frames are used as outputs, as in the H3.6M short-term prediction experiment. As the sequences in this dataset are longer than 144 frames, we also evaluate our model for long-term prediction by estimating the following 60 frames instead of 24.

#### 4.1.2 Evaluation metrics

We report different evaluation metrics in our experiments. The *Euler angle error* metric is a standard metric for motion prediction [2, 22] which we use for both datasets, and is defined as the Euclidean distance between target and predicted Euler angles. The three other metrics are adopted from related pose estimation literature [18, 2, 51]. *Joint angle error* measures the difference in rotation between predicted joint angle and corresponding target rotation at each time-step. *Positional error* calculates the Euclidean distance between the 3D position of each estimated joint compared to the corresponding target position [41, 2]. *Percentage of correct keypoints (PCK)* indicates the fraction of correctly predicted joints within a spherical threshold around the target joint position [29, 45]. For all of the above-mentioned evaluation metrics, we calculate the total values by summing up  $r$  time-steps where for short-term prediction,  $r = 100, 200, 300, 400$  milliseconds, and for long-term prediction  $r = 600, 800, 1000$  milliseconds.

#### 4.1.3 Implementation details

We use ReLU after each of the convolution operations, and a tanh after the FC. All models are trained using Adam optimizer [23] with learning rate 0.0001, weight decay 0.0005,  $\beta_1 = 0.9$ , and  $\beta_2 = 0.999$ . The network is trained with a batch size of 64 on a single NVIDIA TITAN RTX GPU. We train the network for about 50 and 60 epochs for H3.6M and AMASS datasets respectively.

## 4.2. Results

In this section, we report the evaluation results on H3.6M and AMASS datasets. We use zero-Velocity [35], seq2seq [35], SRNN [22], QuaterNet [41], RNN-SPL [2], and RNN (baseline), for comparison. We use a single LSTM cell with 1024 units in the RNN model.

#### 4.2.1 Evaluation on Human3.6M

We compare our model with state-of-the-art methods on four representative activities, including walking, smoking, eating, and discussion for short-term motion prediction. The quantitative comparisons are shown in Table 1, where Euclidean distance between predicted and target ground-truth joint angles in Euler representation is reported as evaluation criteria. It can be observed that our method consistently outperforms the other methods in almost all considered activities. The second best results are yielded by QuaterNet [41] which augments RNNs with quaternion-based normalization and regularization operations.

	Walking				Eating				Smoking				Discussion			
milliseconds	80	160	320	400	80	160	320	400	80	160	320	400	80	160	320	400
Zero-Velocity [35]	0.39	0.68	0.99	1.15	0.27	0.48	0.73	0.86	0.26	0.48	0.97	0.95	0.31	0.67	0.94	1.04
Seq2seq [35]	0.27	0.47	0.70	0.78	0.25	0.43	0.71	0.87	0.33	0.61	1.04	1.19	0.31	0.69	1.03	1.12
SRNN [22]	0.81	0.94	1.16	1.30	0.97	1.14	1.35	1.46	1.45	1.68	1.94	2.08	1.22	1.49	1.83	1.93
QuaterNet [41]	<b>0.21</b>	<b>0.34</b>	<b>0.56</b>	0.62	<b>0.20</b>	0.35	0.58	0.70	0.25	0.47	0.93	<b>0.90</b>	<b>0.26</b>	0.60	<b>0.85</b>	0.93
RNN-SPL [2]	0.26	0.40	0.67	0.78	0.21	0.34	0.55	<b>0.69</b>	0.26	0.48	0.96	0.94	0.30	0.66	0.95	1.05
Ours (MotionFlow)	0.22	<b>0.34</b>	0.57	<b>0.61</b>	<b>0.20</b>	<b>0.33</b>	<b>0.54</b>	0.70	<b>0.23</b>	<b>0.45</b>	<b>0.88</b>	1.01	<b>0.26</b>	<b>0.58</b>	0.86	<b>0.90</b>

Table 1: Prediction results over four representative activities on H3.6M dataset. The results are reported in terms of Euler angle error (smaller is better). The best performance is highlighted in bold. Our method achieves the best performance in most time horizons for all activities.

Short-term prediction (24 frames)																
	Euler				Joint Angle				Positional				PCK (AUC)			
milliseconds	100	200	300	400	100	200	300	400	100	200	300	400	100	200	300	400
Zero-Velocity [35]	1.91	5.93	11.36	17.78	0.37	1.27	2.56	4.11	0.15	0.51	1.05	1.69	0.85	0.82	0.84	0.81
Seq2seq [35]	1.52	<b>3.51</b>	8.92	15.66	0.31	0.72	1.90	3.44	0.12	0.29	0.76	1.41	0.91	0.86	0.86	0.82
RNN	1.69	5.45	10.21	16.31	0.31	1.05	2.19	3.65	0.12	0.42	0.87	1.48	0.89	0.85	0.86	0.83
QuaterNett [41]	1.49	4.70	9.16	14.54	0.26	0.89	1.83	3.00	0.10	0.34	0.71	1.18	0.90	0.87	0.88	0.85
RNN-SPL [2]	1.33	4.15	8.53	12.95	0.22	0.75	1.51	2.60	<b>0.08</b>	0.28	0.61	0.96	<b>0.93</b>	0.90	0.90	0.88
Ours (MotionFlow)	<b>1.11</b>	4.01	<b>7.40</b>	<b>10.10</b>	<b>0.21</b>	<b>0.53</b>	<b>1.11</b>	<b>2.25</b>	<b>0.08</b>	<b>0.22</b>	<b>0.49</b>	<b>0.92</b>	<b>0.93</b>	<b>0.92</b>	<b>0.91</b>	<b>0.89</b>

Long-term prediction (60 frames)												
	Euler			Joint Angle			Positional			PCK (AUC)		
milliseconds	600	800	1000	600	800	1000	600	800	1000	600	800	1000
Zero-Velocity [35]	32.47	49.25	66.65	7.74	11.83	16.13	3.19	4.87	6.64	0.78	0.76	0.74
Seq2seq [35]	36.39	61.60	88.70	9.60	14.77	21.38	3.96	6.02	8.82	0.75	0.71	0.67
RNN	31.25	49.03	69.50	7.34	11.93	17.35	2.96	4.80	6.99	0.78	0.74	0.71
QuaterNett [41]	27.08	41.32	56.66	5.88	9.21	12.84	2.32	3.64	5.09	0.82	0.79	0.77
RNN-SPL [2]	24.44	38.12	53.08	5.04	8.05	11.76	1.95	3.19	4.62	0.84	0.81	0.79
Ours (MotionFlow)	<b>21.60</b>	<b>34.85</b>	<b>51.47</b>	<b>4.42</b>	<b>8.01</b>	<b>11.21</b>	<b>1.75</b>	<b>2.98</b>	<b>4.16</b>	<b>0.85</b>	<b>0.82</b>	<b>0.80</b>

Table 2: Prediction results on AMASS dataset under different evaluation errors (smaller is better) in terms of short-term and long-term motion prediction. The best performance is highlighted in bold. Our method outperforms the-state-of-the-art for all time horizons.

#### 4.2.2 Evaluation on AMASS

We follow the standard protocols used in [2] and evaluate our method in terms of Euler angle, joint angle, positional error, and PCK. We further show the performance of our method for long-term motion prediction where evaluation metrics are calculated by summing up until frame 36, 48 and 60 respectively at 600, 800, and 1000 milliseconds. Table 2 summarizes the results on the AMASS dataset. Our method yields the best results for these different metrics. It is able to consider all observed motions in input frames as motion context, and hence predict the future motion with high fidelity for both short-term and long-term predictions.

#### 4.3. Ablation studies

To evaluate the contribution of different aspects of the proposed method, we conduct ablation studies on both short-term and long-term motion prediction. In particular, we study the impact of (1) inter-frame flows, (2) intra-frame flows, and (3) the structured learning of the output target

in the generative flow modeling (conditioning). Table 3 represents the results of these experiments on the AMASS dataset which is larger and more challenging than H3.6M.

In the first experiment, we assess the impact of inter-frame flows by removing the joint orderings in the condition networks and train the model using the multi-level Glow with 3 levels and 8 steps of the Glow model. The input and output sequences are therefore considered as two 2D matrices of size  $120 \times 135$  consisting of 120 frames. Note that we use a rotation matrix representation with  $R = 9$  for 15 joints. Without explicit ordering of the joints, although the intra-frame joint correspondence are maintained throughout the sequence, all joints are treated equally and the local temporal and spatial dependencies between frames are not suitably learned. This negative effect is more noticeable in the long-term prediction where the highest error is achieved compared to the proposed MotionFlow method. In Table 3, this model is shown where *j-flow* is unchecked.

Next, we add the inter-frame joint orderings back, and this time modify the model by removing the intra-frame

Short-term prediction																		
			Euler				Joint Angle				Positional				PCK (AUC)			
j-flow	s-flow	cond	100	200	300	400	100	200	300	400	100	200	300	400	100	200	300	400
	✓	✓	1.81	5.25	11.22	16.22	0.33	1.00	2.18	3.5	0.15	0.45	0.92	1.53	0.90	0.88	0.87	0.82
✓		✓	1.51	5.84	12.08	18.64	0.35	0.1.17	2.56	3.95	0.13	0.46	0.98	2.13	0.86	0.81	0.79	0.72
✓	✓		2.18	6.11	11.80	18.23	0.41	1.45	2.80	4.25	0.19	0.56	1.27	2.48	0.81	0.78	0.74	0.70
✓	✓	✓	<b>1.11</b>	<b>4.01</b>	<b>7.40</b>	<b>10.10</b>	<b>0.21</b>	<b>0.53</b>	<b>1.11</b>	<b>2.25</b>	<b>0.08</b>	<b>0.22</b>	<b>0.49</b>	<b>0.92</b>	<b>0.93</b>	<b>0.92</b>	<b>0.91</b>	<b>0.89</b>
Long-term prediction																		
			Euler			Joint Angle			Positional			PCK (AUC)						
j-flow	s-flow	cond	600	800	1000	600	800	1000	600	800	1000	600	800	1000	600	800	1000	
	✓	✓	33.48	54.92	73.58	7.12	13.56	18.27	3.48	5.73	8.46	0.76	0.72	0.67				
✓		✓	35.97	58.13	75.33	8.21	14.65	19.94	3.61	5.80	8.63	0.72	0.67	0.61				
✓	✓		36.42	59.77	78.30	8.28	14.74	20.41	3.63	6.04	8.70	0.75	0.71	0.63				
✓	✓	✓	<b>21.60</b>	<b>34.85</b>	<b>51.47</b>	<b>4.42</b>	<b>8.01</b>	<b>11.21</b>	<b>1.75</b>	<b>2.98</b>	<b>4.16</b>	<b>0.85</b>	<b>0.82</b>	<b>0.80</b>				

Table 3: Influence of different aspects of the proposed method under different evaluation metrics on AMASS dataset. joint-dependent flows, sequence-level flows, and conditioning on the input sequence are denoted by ‘j-flow’, ‘s-flow’, and ‘cond’, respectively. They are checked in their corresponding column if they are used in the experiment.

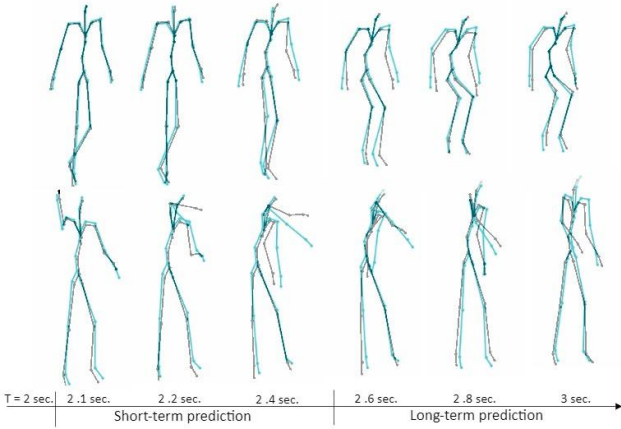


Figure 4: Qualitative analysis of short-term and long-term predictions on two challenging sequences. The predictions (blue) are overlaid with the ground-truth (gray) poses to better visualize the performance. The results demonstrate that MotionFlow predicts both short-term and long-term high-quality motions.

flows. As observed in Table 3 where *s-flow* is unchecked, when we ignore the global smoothness of the frame, the accumulated errors become remarkably larger than our proposed MotionFlow method.

In the final experiment, we remove the conditioning on the input, responsible for structured prediction. We observe that this ablation significantly impacts both short-term and long-term prediction. In particular, this is the case where we achieve the worst results under most metrics. In Table 3, this is shown in the rows where *cond* is unchecked.

#### 4.4. Qualitative results

To visually evaluate our proposed method, we illustrate qualitative comparisons with the state-of-the-art methods,

as shown in Figure 1. Since the Zero-velocity [35] baseline constantly predicts the last observed frame, it is unable to accurately predict complicated sequences even in short-term prediction. Although Seq2seq [35] and RNN-SPL [2] show relatively accurate short-term predictions, they suffer from discontinuities in longer predictions. MotionFlow, however, can generate more precise motions than the other methods since it maintains the temporal consistency of the motion structure in addition to the joint spatial relationships. We further show the qualitative analysis of our method on two challenging sequences. As shown in Figure 4, predictions are close to the ground-truths specially in short-term prediction.

## 5. Conclusion

We propose MotionFlow as a novel generative model for motion prediction. In our approach, we use a novel autoregressive structured prediction representation based on normalizing flows. Our model addresses the issues of maintaining inter-frame and intra-frame structures by leveraging context information in the flow-based representation at two explicit levels. We perform rigorous experiments on two widely used datasets, H3.6M and AMASS and compare the performance of MotionFlow to other methods in the area both quantitatively and qualitatively. Experiments show that our model outperforms the other solutions to set a new state-of-the-art. We believe that the ability for our method to simultaneously learn temporal and spatial relationships provides opportunities to further explore this approach for other similar applications including future event prediction in video sequences.



## References

- [1] Abdelrahman Abdelhamed, Marcus A Brubaker, and Michael S Brown. Noise flow: Noise modeling with conditional normalizing flows. In *Proceedings of the IEEE International Conference on Computer Vision*, pages 3165–3173, 2019. [3](#)
- [2] Emre Aksan, Manuel Kaufmann, and Otmar Hilliges. Structured prediction helps 3d human motion modelling. In *Proceedings of the IEEE International Conference on Computer Vision*, pages 7144–7153, 2019. [1](#), [3](#), [5](#), [6](#), [7](#), [8](#)
- [3] Andrei Atanov, Alexandra Volokhova, Arsenii Ashukha, Ivan Sosnovik, and Dmitry Vetrov. Semi-conditional normalizing flows for semi-supervised learning. *arXiv preprint arXiv:1905.00505*, 2019. [3](#)
- [4] David Belanger and Andrew McCallum. Structured prediction energy networks. In *International Conference on Machine Learning*, pages 983–992, 2016. [2](#), [3](#)
- [5] Yujun Cai, Lin Huang, Yiwei Wang, Tat-Jen Cham, Jianfei Cai, Junsong Yuan, Jun Liu, Xu Yang, Yiheng Zhu, Xiaohui Shen, et al. Learning progressive joint propagation for human motion prediction. In *European Conference on Computer Vision*, pages 226–242. Springer, 2020. [2](#)
- [6] Michael Collins. Discriminative training methods for hidden markov models: Theory and experiments with perceptron algorithms. In *Proceedings of the 2002 conference on empirical methods in natural language processing (EMNLP 2002)*, pages 1–8, 2002. [2](#)
- [7] Fernando De la Torre, Jessica Hodgins, Adam Bargteil, Xavier Martin, Justin Macey, Alex Collado, and Pep Beltran. Guide to the carnegie mellon university multimodal activity (cmu-mmact) database. 2009. [6](#)
- [8] Laurent Dinh, David Krueger, and Yoshua Bengio. Nice: Non-linear independent components estimation. *arXiv preprint arXiv:1410.8516*, 2014. [3](#)
- [9] Laurent Dinh, Jascha Sohl-Dickstein, and Samy Bengio. Density estimation using real nvp. *arXiv preprint arXiv:1605.08803*, 2016. [3](#), [11](#)
- [10] Yong Du, Wei Wang, and Liang Wang. Hierarchical recurrent neural network for skeleton based action recognition. In *Proceedings of the IEEE conference on computer vision and pattern recognition*, pages 1110–1118, 2015. [2](#)
- [11] Basura Fernando, Efstratios Gavves, Jose M Oramas, Amir Ghodrati, and Tinne Tuytelaars. Modeling video evolution for action recognition. In *Proceedings of the IEEE Conference on Computer Vision and Pattern Recognition*, pages 5378–5387, 2015. [2](#)
- [12] Colin Graber, Ofer Meshi, and Alexander Schwing. Deep structured prediction with nonlinear output transformations. *Advances in Neural Information Processing Systems*, 31:6320–6331, 2018. [2](#), [3](#)
- [13] Colin Graber and Alexander Schwing. Graph structured prediction energy networks. *arXiv preprint arXiv:1910.14670*, 2019. [3](#)
- [14] Liang-Yan Gui, Yu-Xiong Wang, Xiaodan Liang, and José MF Moura. Adversarial geometry-aware human motion prediction. In *Proceedings of the European Conference on Computer Vision (ECCV)*, pages 786–803, 2018. [1](#), [2](#)
- [15] Tamir Hazan and Raquel Urtasun. A primal-dual message-passing algorithm for approximated large scale structured prediction. In *Advances in neural information processing systems*, pages 838–846, 2010. [3](#)
- [16] Jonathan Ho, Xi Chen, Aravind Srinivas, Yan Duan, and Pieter Abbeel. Flow++: Improving flow-based generative models with variational dequantization and architecture design. In *International Conference on Machine Learning*, pages 2722–2730. PMLR, 2019. [2](#), [3](#)
- [17] Emiel Hooeboom, Rianne Van Den Berg, and Max Welling. Emerging convolutions for generative normalizing flows. In *International Conference on Machine Learning*, pages 2771–2780, 2019. [3](#)
- [18] Yinghao Huang, Manuel Kaufmann, Emre Aksan, Michael J Black, Otmar Hilliges, and Gerard Pons-Moll. Deep inertial poser: Learning to reconstruct human pose from sparse inertial measurements in real time. *ACM Transactions on Graphics (TOG)*, 37(6):1–15, 2018. [6](#)
- [19] Sergey Ioffe and Christian Szegedy. Batch normalization: Accelerating deep network training by reducing internal covariate shift. In *International Conference on Machine Learning*, pages 448–456, 2015. [11](#)
- [20] Catalin Ionescu, Dragos Papava, Vlad Olaru, and Cristian Sminchisescu. Human3.6m: Large scale datasets and predictive methods for 3d human sensing in natural environments. *IEEE transactions on pattern analysis and machine intelligence*, 36(7):1325–1339, 2013. [2](#), [6](#)
- [21] Ajay Jain, Pieter Abbeel, and Deepak Pathak. Locally masked convolution for autoregressive models. In *Conference on Uncertainty in Artificial Intelligence*, pages 1358–1367. PMLR, 2020. [11](#)
- [22] Ashesh Jain, Amir R Zamir, Silvio Savarese, and Ashutosh Saxena. Structural-rnn: Deep learning on spatio-temporal graphs. In *Proceedings of the IEEE conference on computer vision and pattern recognition*, pages 5308–5317, 2016. [6](#), [7](#)
- [23] Diederik P Kingma and Jimmy Ba. Adam: A method for stochastic optimization. *arXiv preprint arXiv:1412.6980*, 2014. [6](#)
- [24] Durk P Kingma and Prafulla Dhariwal. Glow: Generative flow with invertible 1x1 convolutions. In *Advances in neural information processing systems*, pages 10215–10224, 2018. [2](#), [3](#), [5](#)
- [25] Diederik P Kingma, Tim Salimans, Rafal Jozefowicz, Xi Chen, Ilya Sutskever, and Max Welling. Improving variational inference with inverse autoregressive flow. *arXiv preprint arXiv:1606.04934*, 2016. [2](#)
- [26] Ivan Kobyzev, Simon Prince, and Marcus Brubaker. Normalizing flows: An introduction and review of current methods. *IEEE Transactions on Pattern Analysis and Machine Intelligence*, 2020. [2](#), [3](#), [4](#)
- [27] M. Kumar, M. Babaeizadeh, D. Erhan, Chelsea Finn, S. Levine, Laurent Dinh, and Durk Kingma. Videoflow: A flow-based generative model for video. *ArXiv*, abs/1903.01434, 2019. [3](#)
- [28] Kyoungoh Lee, Inwoong Lee, and Sanghoon Lee. Propagating lstm: 3d pose estimation based on joint interdependency. In *Proceedings of the European Conference on Computer Vision (ECCV)*, pages 119–135, 2018. [2](#)

- [29] Chi Li, Jin Bai, and Gregory D Hager. A unified framework for multi-view multi-class object pose estimation. In *Proceedings of the European Conference on Computer Vision (ECCV)*, pages 254–269, 2018. 6
- [30] Zhenguang Liu, Shuang Wu, Shuyuan Jin, Qi Liu, Shijian Lu, Roger Zimmermann, and Li Cheng. Towards natural and accurate future motion prediction of humans and animals. In *Proceedings of the IEEE Conference on Computer Vision and Pattern Recognition*, pages 10004–10012, 2019. 5
- [31] Matthew Loper, Naureen Mahmood, Javier Romero, Gerard Pons-Moll, and Michael J Black. Smpl: A skinned multi-person linear model. *ACM transactions on graphics (TOG)*, 34(6):1–16, 2015. 6
- [32] You Lu and Bert Huang. Structured output learning with conditional generative flows. In *AAAI*, pages 5005–5012, 2020. 2, 4, 5, 13
- [33] Naureen Mahmood, Nima Ghorbani, Nikolaus F Troje, Gerard Pons-Moll, and Michael J Black. Amass: Archive of motion capture as surface shapes. In *Proceedings of the IEEE International Conference on Computer Vision*, pages 5442–5451, 2019. 1, 2, 6
- [34] Wei Mao, Miaomiao Liu, Mathieu Salzmann, and Hongdong Li. Learning trajectory dependencies for human motion prediction. In *Proceedings of the IEEE/CVF International Conference on Computer Vision*, pages 9489–9497, 2019. 2
- [35] Julieta Martinez, Michael J Black, and Javier Romero. On human motion prediction using recurrent neural networks. In *Proceedings of the IEEE Conference on Computer Vision and Pattern Recognition*, pages 2891–2900, 2017. 1, 2, 6, 7, 8
- [36] Joe Yue-Hei Ng, Jonghyun Choi, Jan Neumann, and Larry S Davis. Actionflownet: Learning motion representation for action recognition. In *2018 IEEE Winter Conference on Applications of Computer Vision (WACV)*, pages 1616–1624. IEEE, 2018. 2
- [37] Vlad Niculae, André FT Martins, Mathieu Blondel, and Claire Cardie. Sparsemap: Differentiable sparse structured inference. *arXiv preprint arXiv:1802.04223*, 2018. 3
- [38] Sebastian Nowozin and Christoph H Lampert. *Structured learning and prediction in computer vision*, volume 6. Now publishers Inc, 2011. 3
- [39] Aaron van den Oord, Nal Kalchbrenner, Oriol Vinyals, Lasse Espeholt, Alex Graves, and Koray Kavukcuoglu. Conditional image generation with pixelcnn decoders. *arXiv preprint arXiv:1606.05328*, 2016. 5
- [40] George Papamakarios, Theo Pavlakou, and Iain Murray. Masked autoregressive flow for density estimation. *arXiv preprint arXiv:1705.07057*, 2017. 2
- [41] Dario Pavllo, David Grangier, and Michael Auli. Quaternion: A quaternion-based recurrent model for human motion. *arXiv preprint arXiv:1805.06485*, 2018. 5, 6, 7
- [42] Danilo Rezende and Shakir Mohamed. Variational inference with normalizing flows. In *International Conference on Machine Learning*, pages 1530–1538. PMLR, 2015. 3
- [43] Amir Shahroudy, Jun Liu, Tian-Tsong Ng, and Gang Wang. Ntu rgb+ d: A large scale dataset for 3d human activity analysis. In *Proceedings of the IEEE conference on computer vision and pattern recognition*, pages 1010–1019, 2016. 2
- [44] Leonid Sigal, Alexandru O Balan, and Michael J Black. Humaneva: Synchronized video and motion capture dataset and baseline algorithm for evaluation of articulated human motion. *International journal of computer vision*, 87(1-2):4, 2010. 6
- [45] Adrian Spurr, Jie Song, Seonwook Park, and Otmar Hilliges. Cross-modal deep variational hand pose estimation. In *Proceedings of the IEEE Conference on Computer Vision and Pattern Recognition*, pages 89–98, 2018. 6
- [46] Charles Sutton and Andrew McCallum. An introduction to conditional random fields for relational learning. *Introduction to statistical relational learning*, 2:93–128, 2006. 2
- [47] Bugra Tekin, Isinsu Katircioglu, Mathieu Salzmann, Vincent Lepetit, and Pascal Fua. Structured prediction of 3d human pose with deep neural networks. *arXiv preprint arXiv:1605.05180*, 2016. 2
- [48] Brian L Trippe and Richard E Turner. Conditional density estimation with bayesian normalising flows. *arXiv preprint arXiv:1802.04908*, 2018. 4
- [49] Ioannis Tsochantaridis, Thomas Hofmann, Thorsten Joachims, and Yasemin Altun. Support vector machine learning for interdependent and structured output spaces. In *Proceedings of the twenty-first international conference on Machine learning*, page 104, 2004. 2
- [50] Lifu Tu and Kevin Gimpel. Learning approximate inference networks for structured prediction. *arXiv preprint arXiv:1803.03376*, 2018. 2, 3
- [51] Timo Von Marcard, Bodo Rosenhahn, Michael J Black, and Gerard Pons-Moll. Sparse inertial poser: Automatic 3d human pose estimation from sparse imus. In *Computer Graphics Forum*, volume 36, pages 349–360. Wiley Online Library, 2017. 6
- [52] Jiang Wang, Zicheng Liu, Ying Wu, and Junsong Yuan. Mining actionlet ensemble for action recognition with depth cameras. In *2012 IEEE Conference on Computer Vision and Pattern Recognition*, pages 1290–1297. IEEE, 2012. 2
- [53] Pichao Wang, Wanqing Li, Chuankun Li, and Yonghong Hou. Action recognition based on joint trajectory maps with convolutional neural networks. *Knowledge-Based Systems*, 158:43–53, 2018. 2
- [54] Fisher Yu and Vladlen Koltun. Multi-scale context aggregation by dilated convolutions. *arXiv preprint arXiv:1511.07122*, 2015. 11
- [55] Wentao Zhu, Cuiling Lan, Junliang Xing, Wenjun Zeng, Yanghao Li, Li Shen, and Xiaohui Xie. Co-occurrence feature learning for skeleton based action recognition using regularized deep lstm networks. *arXiv preprint arXiv:1603.07772*, 2016. 1, 2
- [56] Zachary Ziegler and Alexander Rush. Latent normalizing flows for discrete sequences. In *International Conference on Machine Learning*, pages 7673–7682. PMLR, 2019. 2

## 6. Appendix

We provide more detailed descriptions of our method and additional experiments, which could not be included in the main paper due to constraints in space.

### 6.1. Architecture details

Figure 5 represents our model architecture. We use a multi-scale architecture [9] to combine the steps of the normalizing flow. It includes a squeeze layer to shuffle the variables and a split layer to reduce the computation costs. Each step of the normalizing flow consists of *actnorm*, *invertible*  $1 \times 1$  *convolution*, and *affine coupling* layers.

Let the input and output of each layer be respectively denoted as  $\alpha$  and  $\beta$ . We define the shape of each layer by  $[h \times w \times c]$ . The spatial and channel dimensions are then respectively denoted as  $[h, w]$  and  $c$ .

In the *actnorm* layer, scale and bias parameters of each channel are used to perform an affine transformation of the activations. This operation is similar to batch normalization [19], which stabilizes the training of the network consisting of multiple flow operations. It is defined as:

$$\beta_{i,j} = s \odot \alpha_{i,j} + b, \quad (7)$$

where  $(i, j)$  denote the spatial indices into tensors  $\alpha$  and  $\beta$ , operator  $\odot$  is the element-wise product, and  $s$  and  $b$  are two  $1 \times c$  vector parameters denoting the scale and the bias. In our method, we use an autoregressive network (represented as  $CONV_1 + FC_1$  in Figure 5) on the input sequence to generate these two vectors.

The *actnorm* layer is followed by an *invertible*  $1 \times 1$  *convolutional* layer which generalizes the permutation operation. It allows learnable reordering of channels in the input layer by incorporating a permutation along the channel dimension. It is defined as:

$$\beta_{i,j} = W \alpha_{i,j}, \quad (8)$$

where  $W$  denotes a  $c \times c$  weight matrix. We initialize this matrix by using an autoregressive network (represented as  $CONV_1 + FC_2$  in Figure 5) on the input sequence.

An *affine coupling* layer finally captures the correlations among spatial dimensions. It splits the input variables along the channel dimension into two halves, *i.e.*,  $\alpha_1$  and  $\alpha_2$ . It then adds a learned transformation of one half to the other half. More specifically, we use  $CONV_2 + CONV_3$  to extract the autoregressive features from input sequence  $x$  and concatenate them to  $\alpha_1$ . This creates  $h$  which is used in  $CONV_2$  to generate  $s_2$ , and  $b_2$  parameters for  $\alpha_2$  to build  $\beta_2$ . The output of this layer is finally obtained by concate-

nating  $\alpha_1$  and  $\beta_2$ . These operations are formulated as:

$$\begin{aligned} \alpha_1, \alpha_2 &= \text{split}(\alpha), \\ h &= \text{concat}(\alpha_1, CONV_2(x)), \\ s_2, b_2 &= CONV_3(h), \\ \beta_2 &= s_2 \odot \alpha_2 + b_2, \\ \beta &= \text{concat}(\alpha_1, \beta_2), \end{aligned} \quad (9)$$

where  $\text{split}()$  and  $\text{concat}()$  perform operations along the channel dimension. The size of the  $s_2$  and  $b_2$  vectors is the same as that of  $\beta_2$ .

In the following, we further describe the networks used in MotionFlow, that provide autoregressive inter- and intra-frame features in specific orderings. Each of the convolutional layers  $CONV_1$  and  $CONV_2$  consists of autoregressive neural networks implemented with two convolutional sets. It must be noted that the input to these layers is a motion sequence  $x$  of length  $(t - 1)$  represented as a  $[3 \times ((t - 1)/3) \times (J \times H)]$  matrix, where  $J$  is the number of joints in each frame and  $H$  denotes the dimensionality of the per joint representation.

There are two autoregressive networks with two different masks in each of the  $CONV_1$  and  $CONV_2$ . Figure 6 illustrates two sets of kernel masks for two different orderings. One set of masks conditions on the joint positions in the current frame (which follows the kinematic chain ordering) and another one conditions on the positions of the current joint in the previous frames. Figure 6 (a)-(c) and Figure 6 (d)-(f) show kernel masks in the first and second sets, respectively. The shape of the mask for a  $[w \times h]$  layer is  $[(3 * 3) \times (w * h)]$ . These masks are separately applied on the convolutions at each network ensuring that they use information about the joints in the provided orderings. Otherwise, the conditional distribution would be violated. Each autoregressive network comprises three convolution operations. One convolution operates on the input, and the other two convolutions use undilated and dilated kernel masks for the other layers. The kernel size for all three convolutions is  $(3 \times 3)$ . The only difference in two autoregressive networks is their masks which correspond to different orderings.

We use dilated convolutions [54, 21] since they expand the receptive field without limiting the orderings. Thus, we prefer them in contrast to using downsampling which causes information loss and prevents the accurate ordering.

The outputs of the two autoregressive networks are combined and fed to the fully connected layers. We use  $FC_1$  for the *actnorm* layer and  $FC_2$  for the *invertible*  $1 \times 1$  convolutional layer. The output channels in  $FC_1$  and  $FC_2$  depend on the size of  $z_L$  which is different in every level of the multi-scale flow.

As shown in Figure 5 and Eq. 9, the network  $CONV_3$  builds the scale and bias parameters for the affine coupling layer. It includes three convolution operations with-

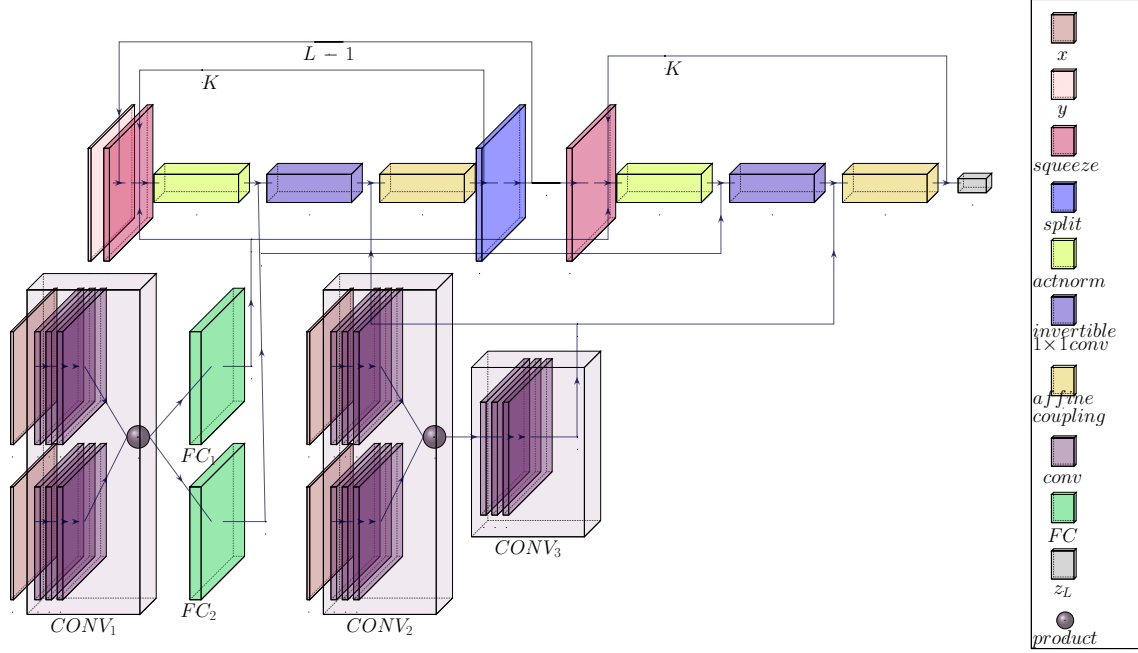


Figure 5: An overview of the MotionFlow. The generation procedure of the high-dimensional output sequence in the latent space is leveraged with the input motion sequence. The autoregressive inter- and intra-frame spatio-temporal features are extracted from the input sequence.

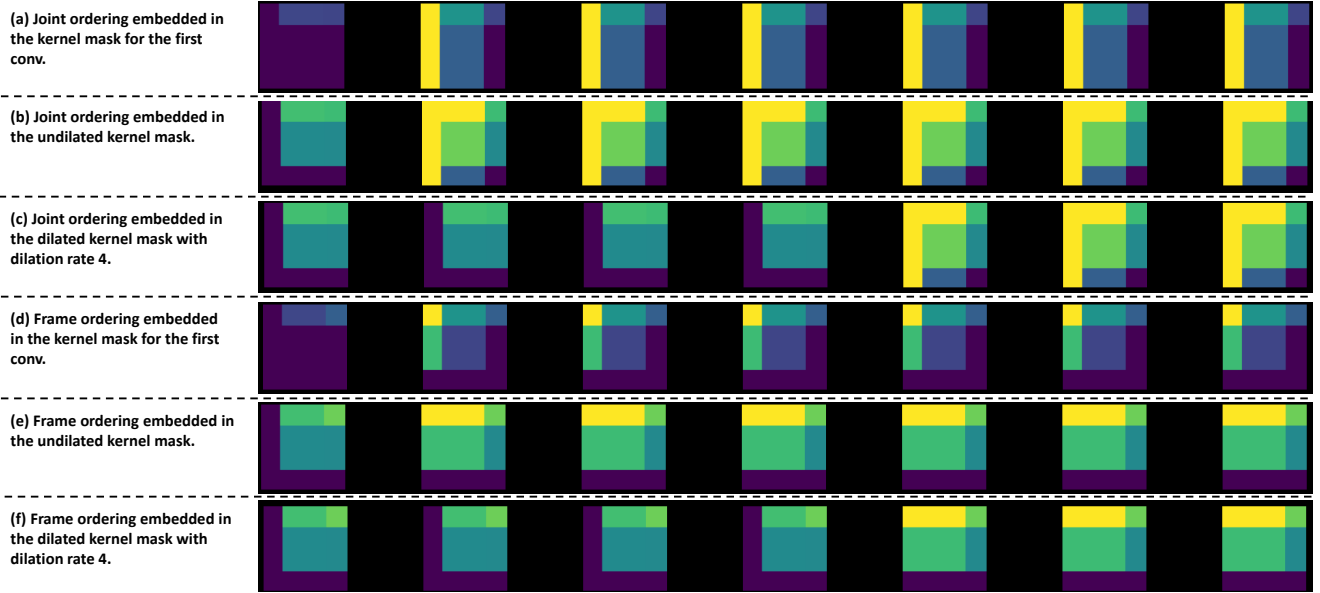


Figure 6: Kernel masks for two different orderings. (a)-(c) show the intra-frame ordering embedded in three masks. (d)-(f) represent three masks for inter-frame ordering. The first mask is applied on the first convolution, and the other two masks are used in the other convolutions.

out masking. The channel size for the first one is equal to the output channel in the last convolution in the  $CONV_2$ . The output channel is equal to  $2 * size(z_L)$ . See Table 4 for

details.

By using masks in different ordering and stacking multiple autoregressive layers, our model can capture large re-



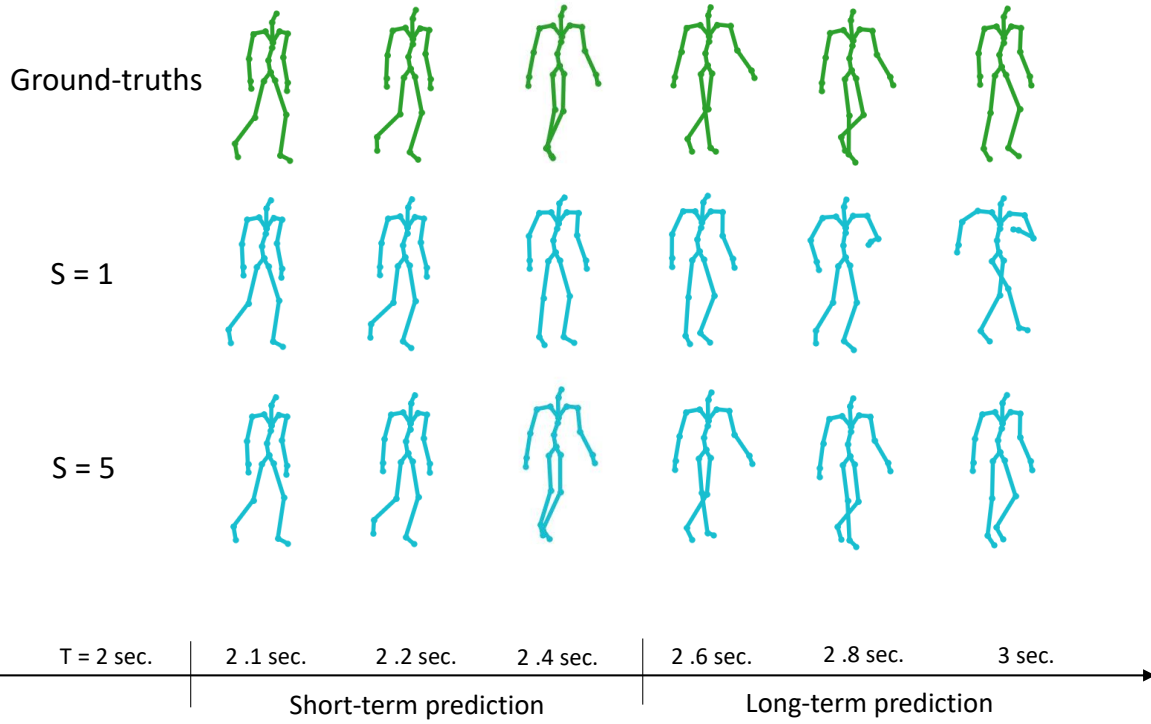


Figure 7: Effect of sampled-based inference. The first row shows ground truth motions, the second and third rows represent predicted motions using different number of samples which is respectively 1 and 5.

ceptive fields, and explore joint correlations in both the spatial and temporal dimensions.

## 6.2. Sampled-based prediction

We conduct more experiments to show the effectiveness of the sample-based inference in our method. Instead of using a gradient-based optimization such as gradient descent method to optimize  $y$ , we use a sample-based technique [32] for inference. The number of samples  $S$  is a hyperparameter that is set empirically. Based on our experiments, we observe that by choosing the number of samples as 5, we can achieve optimal results with a high quality prediction. When  $S > 1$ , we average all predicted motions for the final prediction.

As illustrated in Figure 7, the predictions at  $S = 5$  show significant improvement compared to  $S = 1$ . This is because the average of the predicted motions for different samples smooths the motions at longer term and makes the prediction more robust.

	Type	Kernel	Channel	Masked	Kernel type
$CONV_1$ (autoregressive 1)	Conv 2d	$3 \times 3$	16	✓	initial
	Conv 2d	$3 \times 3$	16	✓	undilated
	Conv 2d	$3 \times 3$	2	✓	dilated
$CONV_1$ (autoregressive 2)	Conv 2d	$3 \times 3$	16	✓	initial
	Conv 2d	$3 \times 3$	16	✓	undilated
	Conv 2d	$3 \times 3$	2	✓	dilated
$FC_1$	Linear	-	32	-	-
	Linear	-	32	-	-
	Linear	-	$(2 \times size(z_L))$	-	-
$FC_2$	Linear	-	32	-	-
	Linear	-	32	-	-
	Linear	-	$(2 \times size(z_L))^2$	-	-
$CONV_2$ (autoregressive 1)	Conv 2d	$3 \times 3$	16	✓	initial
	Conv 2d	$3 \times 3$	16	✓	undilated
	Conv 2d	$3 \times 3$	$(size(z_L))$	✓	dilated
$CONV_2$ (autoregressive 2)	Conv 2d	$3 \times 3$	16	✓	initial
	Conv 2d	$3 \times 3$	16	✓	undilated
	Conv 2d	$3 \times 3$	$(size(z_L))$	✓	dilated
$CONV_3$	Conv 2d	$3 \times 3$	256	-	-
	Conv 2d	$1 \times 1$	256	-	-
	Conv 2d	$3 \times 3$	$(2 \times size(z_L))$	-	-

Table 4: Network parameters of the MotionFlow architecture.